WELDING RESEARCH

SUPPLEMENT TO THE *WELDING JOURNAL*, DECEMBER 1998
Sponsored by the American Welding Society and the Welding Research Council

Microstructure/Property Relationships in Dissimilar Welds between Duplex Stainless Steels and Carbon Steels

The effect of weld metal microstructure on toughness and pitting corrosion resistance is evaluated for both a duplex stainless steel and Ni-based filler metal

BY E. J. BARNHOUSE AND J. C. LIPPOLD

ABSTRACT. The metallurgical characteristics, toughness and corrosion resistance of dissimilar welds between duplex stainless steel Alloy 2205 and carbon steel A36 have been evaluated. Both duplex stainless steel ER2209 and Ni-based Alloy 625 filler metals were used to join this combination using a multipass, gas tungsten arc welding (GTAW) process. Defect-free welds were made with each filler metal. The toughness of both the 625 and 2209 deposits were acceptable, regardless of heat input. A narrow martensitic region with high hardness was observed along the A36/2209 fusion boundary. A similar region was not observed in welds made with the 625 filler metal. The corrosion resistance of the welds made with 2209 filler metal improved with increasing heat input, probably due to higher levels of austenite and reduced chromium nitride precipitation. Welds made with 625 exhibited severe attack in the root pass, while the bulk of the weld was resistant. This investigation has shown that both filler metals can be used to join carbon steel to duplex stainless steels, but that special precautions may be necessary in corrosive environments.

Introduction

Duplex stainless steels have become increasingly attractive to a number of industry sectors due to their superior mechanical properties and corrosion characteristics relative to other stainless steels and structural steels. Although the joining of duplex stainless steels to themselves has been studied extensively, the increased application of these steels will require a better understanding of the issues associated with welds to dissimilar metals. The joining of dissimilar materials is generally more challenging than that of similar materials because of differences in the physical, mechanical and metallurgical properties of the base metals to be joined. These differences may also complicate the selection of filler metals compatible to both base metals. Therefore, filler metal selection is often a compromise between the two dissimilar metals. There are few guidelines for dissimilar metal joining and, in most cases, predicting the microstructure and resultant properties of the weld deposit can be difficult.

E. J. BARNHOUSE is with Weirton Steel Corp., Weirton, W. Va. J. C. LIPPOLD is with The Ohio State University, Columbus, Ohio.

KEY WORDS

Duplex Stainless
Alloy 625
Dissimilar Metals
Corrosion Resistance
Constitutions Diagrams
Ferrite Number
Filler Metal
Carbon Steel

This study was designed to provide some insight into the microstructure/property relationships in dissimilar fusion welds with duplex stainless steels. The dissimilar materials selected for the overall study included a plain carbon structural steel (A36), an austenitic stainless steel (Type 304L) and a martensitic stainless steel (Type 410). This report focuses on the dissimilar combination of Alloy 2205 and A36. A future paper will report the results of studies conducted on the other combinations.

Stainless Steel/Carbon Steel Dissimilar Joints

Early investigations on the joining of dissimilar metals were primarily devoted to ferrous alloys; however, much of the emphasis was placed on the prevention of weld metal liquation cracking (often referred to as microfissuring), heat-affected zone cracking, carbon migration and oxide penetration, as discussed by Pattee, *et al.* (Ref. 1). In the 1940s, Schaeffler proposed a diagram for the selection of electrodes for the dissimilar joining of plain carbon and stainless steels that related the microstructural constitution of the weld deposit to its composition, as dictated by the relative proportion of filler metals and base metals (Ref. 2). This diagram (Fig. 1), commonly referred to as the Schaeffler Constitution Diagram, can be used as a means of predicting the weld metal microstructure of dissimilar metal welds in a select group of alloys. By plotting the Cr- and Ni-equivalents for the materials on

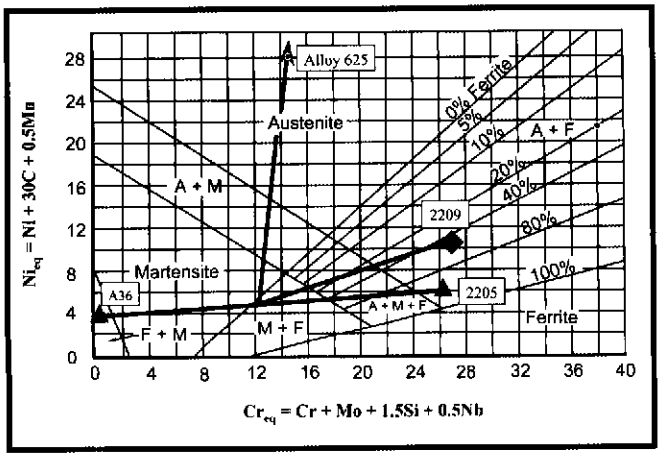

Fig. 1 — Schaeffler Diagram (Ref. 2) showing the dissimilar combinations used in this investigation.

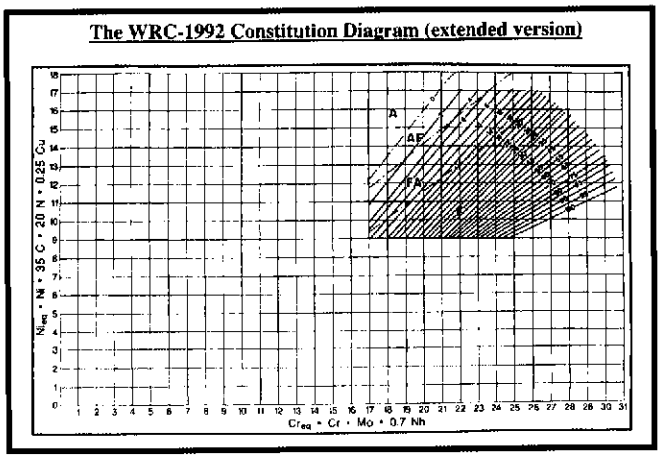

Fig. 2 — WRC-1992 diagram, extended version (Ref. 5).

Table 1 — Fusion Zone Mechanical Properties of Dissimilar Joints with Alloy 2507 (Ref. 6)

Property	2507/ Carbon Steel	2507/316
Tensile Strength, ksi	61.8	85.1
Yield Strength, ksi	43.4	54.5
Elongation, %	23	45

Table 2 — Chemical Composition and Cr_{eq} and Ni_{eq} of the Base and Filler Metals (wt-%)

Element	Alloy 2205	A36	ER2209	ERNiCrMo-3
Cr	22.16		22.71	21.84
Ni	5.64		8.23	64.46
Mo	3.04		3.18	8.91
Mn	1.46	0.627	1.64	0.02
Si	0.48	0.236	0.52	0.03
C	0.014	0.088	0.015	0.030
N	0.18		0.160	
S	0.001	0.025	0.001	< 0.001
P	0.028	0.005	0.020	0.003
Fe	bal.	bal.	bal.	bal.
Cr_{eq}[a]	25.20	—	25.89	33.15
Ni_{eq}[b]	9.73	—	11.98	65.51
Cr_{eq}/Ni_{eq}	2.59	—	2.16	0.51
Q factor[c]	2.19	—	1.66	0.27
PRE[d]	35.07	—	35.76	51.24

(a) Cr + Mo + 0.7Nb, WRC-1992.
(b) Ni + 20N + 35C + 0.25Cu, WRC-1992.
(c) (Cr + 1.5Mo + 2Mn + 0.25Si)/(2Ni + 12C + 12N).
(d) PRE (Pitting Resistance Equivalent) = Cr + 3.3(Mo + 0.5W) + 16N.

the diagram and connecting the base metals by a tie line, the deposit microstructure can be estimated by connecting a point along that tie line (selected as the midpoint in Fig. 1) to a tie line to the filler metal composition. The weld metal constitution then lies along the line between the filler metal and base metal midpoint as dictated by the level of dilution.

The ability to predict microstructure using the Schaeffler Diagram provided a valuable tool for the selection of filler metals and the determination of the effects of base metal dilution. The diagram was particularly useful for predicting the ferrite content in austenitic stainless steel deposits and determining the constitution of dissimilar combinations of carbon steels and austenitic stainless steels.

The Schaeffler Diagram does not have a specific weighting factor for nitrogen, however, and as a result, a diagram was proposed by DeLong in 1974 that incorporated N in the Ni-equivalent formula (Ref. 3). This diagram allowed for more accurate estimation of ferrite content over a narrower composition range than the Schaeffler Diagram, improving and correcting the limitations associated with the Schaeffler Diagram. The DeLong Diagram was later found to misrepresent Mn, and FN (Ferrite Number) predictions of highly alloyed compositions such as 309 stainless steel were found to be inaccurate (Ref. 4). Furthermore, its limited composition range made it difficult to utilize for dissimilar metal welding.

Siewert, *et al.* (Ref. 4), developed a modified prediction diagram called the WRC-1988 diagram. This diagram modified and greatly simplified the Cr- and Ni-equivalent formulae and corrected the overestimation of FN for higher alloyed weld metals. Recently, Kotecki, *et al.* (Ref. 5), had shown Cu to influence the austenite formation and therefore added a Cu factor in the Ni-equivalent formula. This change resulted in the WRC-1992 diagram, which is essentially identical to the WRC-1988 with the addition of a Cu factor in Ni-equivalent formula. An extended version of this diagram (Fig. 2) allows FN estimation in dissimilar welds but does not contain other constitution regimes, as in the Schaeffler Diagram.

Duplex Stainless Steel to Carbon Steel

Recently, Odegard, *et al.* (Ref. 6), studied the joining of duplex Alloy SAF 2507 to carbon steels with respect to fusion zone mechanical properties. They reported that the phase stability and the overall properties of the fusion zone were influenced by the welding parameters and that low heat inputs were necessary to ensure structural integrity and solidification cracking resistance. Furthermore, they noted that a highly ferritic fusion zone resulted from high dilution by the carbon steel, making the weld metal microstructure susceptible to secondary austenite formation in multipass welding due to reheating of the deposited weld metal by subsequent passes. High heat input welding schedules were reported to

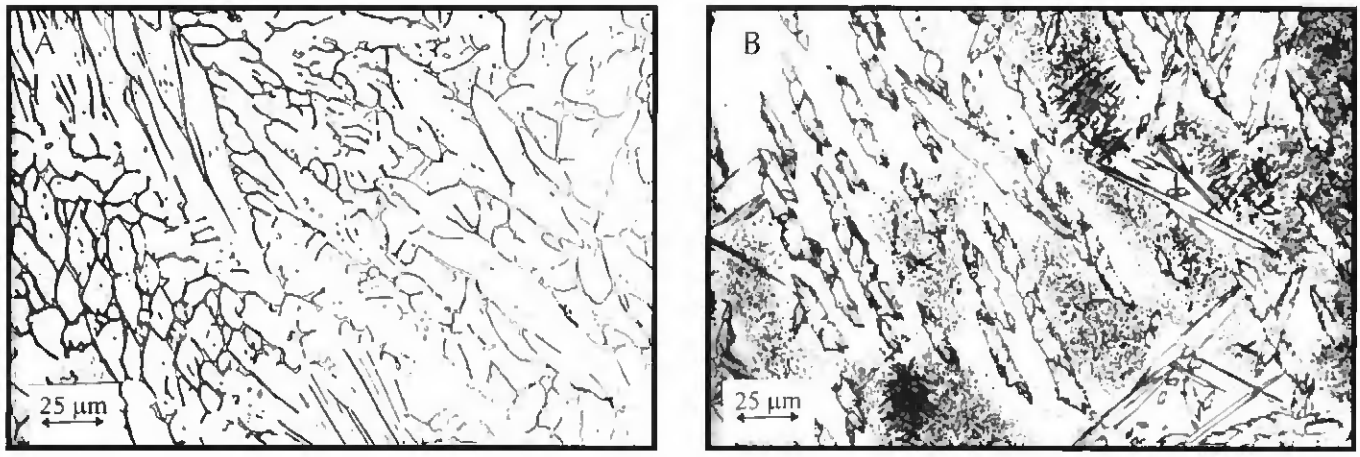

Fig. 3 — Cross section of 2205/2209/A36 weld combination: A — Root pass; B — cover pass.

increase the susceptibility to fusion zone solidification cracking.

Table 1 presents mechanical property data, collected by Odegard, *et al.* (Ref. 6), which includes tensile strength, yield strength and elongation values for dissimilar joints between the super-duplex Alloy 2507 and either carbon steel or Type 316 austenitic stainless steel. No other mechanical property data for dissimilar welds between duplex stainless steels and carbon steels was found in the literature.

Experimental Procedure

Materials

Welding trials were designed to study the dissimilar joining of duplex stainless steel Alloy 2205 to A36 carbon steel. This dissimilar combination was selected based on a survey of industrial users. Both duplex stainless steel and Ni-based filler metals were selected to join these metals. The chemical compositions for the base and filler metals are listed in Table 2. The base materials were supplied in the form of 12.5-mm (0.5-in.) plate. These plates were cut into 5 x 20 cm (2 x 7.8 in.) coupons with a 37-deg bevel on each plate to provide a 74-deg groove angle for a single-V-groove butt joint configuration. The root face was 1.6 to 2.4 mm (0.062 to 0.094 in.) with a root opening of 2.4 mm.

Welding Procedure

All welding was performed using the automatic gas tungsten arc welding (GTAW) process with cold wire feed of 1.14-mm (0.045-in.) diameter welding wire. ER2209 and Alloy 625 filler metals were used in the multipass welds to join duplex Alloy 2205 to A36 carbon steel. Two heat input levels were initially selected and used throughout the study, as listed in Table 3. The welding heat inputs used were 1.57 kJ/mm (39.8 kJ/in.) and 2.60 kJ/mm (66 kJ/in.), with the only exception being the root passes in each combination. Due to the difference in material properties (mainly thermal conductivity) the heat flow differed between the two filler metals, thus the root pass heat inputs were different. The 2205/2209/A36 combination utilized a root pass heat input of 1.05 kJ/mm (26.7 kJ/in.), while that of the 2205/625/A36 combination was 1.90 kJ/mm (48.3 kJ/in.).

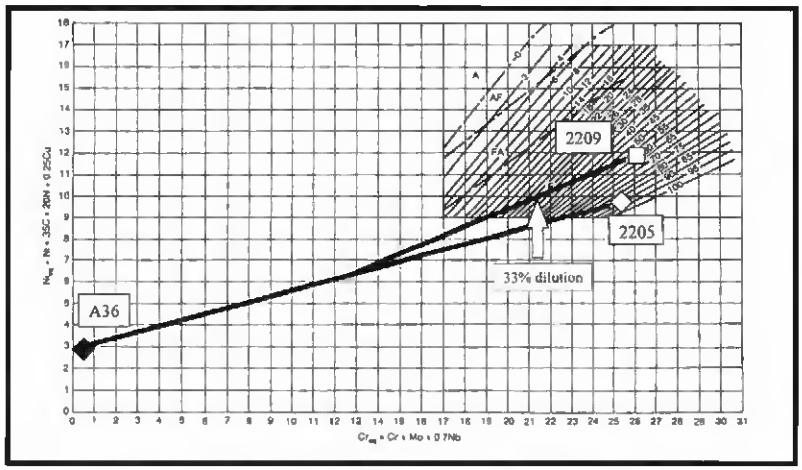

Fig. 4 — WRC-1992 diagram for A36/2209/2205 combination.

Metallurgical Characterization

Optical Metallography

Weld cross sections were removed from each of the combinations and polished through 0.05-micron alumina. The samples were electrolytically etched in 10% oxalic acid at 5–7 V for 20–25 s. Also, color etching techniques were employed to provide better resolution between the ferrite and austenite. These techniques included a two-step modified Murakami's etch (Ref. 7), which produces a composition-sensitive film resulting in a variety of colors on the ferrite phase, while the austenite remains white (uncolored). A ferro-fluid colloidal suspension of Fe_3O_4 was also used to reveal the duplex microstructure (Ref. 7). Residual magnetism attracts Fe_3O_4 particles to the ferrite phase to provide a color of brown or dark blue in stark contrast to the austenite, which is white.

Microhardness Surveys

Hardness testing was carried out on a Leco Model M-400 microhardness unit using a 1-kg load. Surveys were conducted both across the weld and from root to cover pass within the weld deposit. The distance between indents was determined by the weld dimensions in order to obtain appropriate data for each

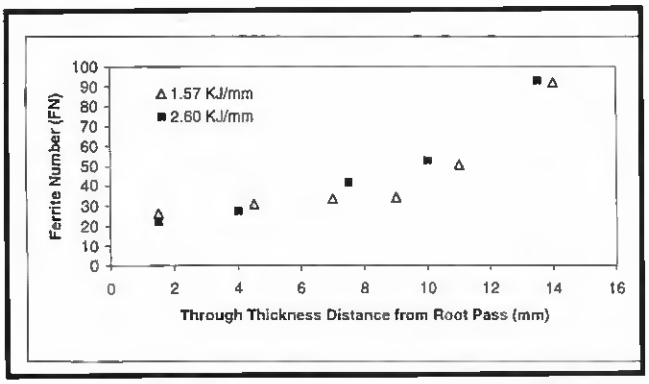

Fig. 5 — FN vs. location for the 2205/2209/A36 weld combination.

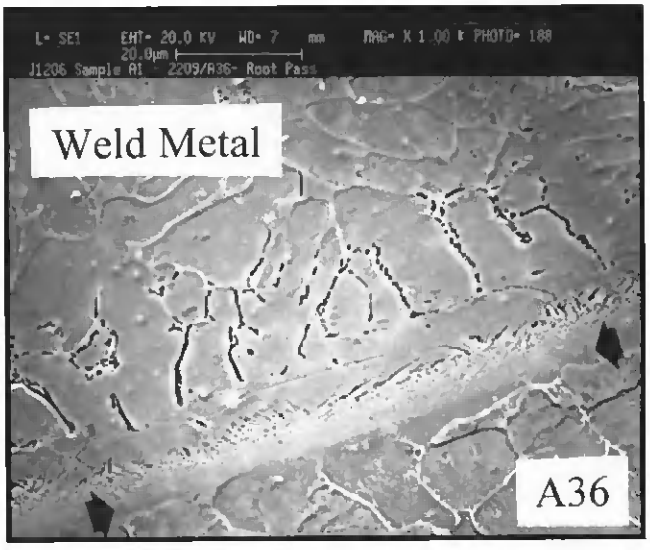

Fig. 6 — Representative micrograph of 2209/A36 fusion boundary region. Arrows indicate fusion boundary.

Table 3 — GTAW Process Parameters

	Low Heat Input, 1.57 kJ/mm	High Heat Input, 2.60 kJ/mm
Voltage	10 V	11 V
Current	200 A	300 A
Travel speed	3.0 in./min (1.27 mm/s)	3.0 in./min (1.27 mm/s)
Wire feed speed	33 in./min (13.97 mm/s)	50 in./min (21.17 mm/s)
Interpass temp., max	150°C	150°C

Table 4 — FN and Hardness for the Fusion Zone and Boundary Region

Combination	Root Pass FN	Root Pass DPH	Fill Pass FN	Fill Pass DPH	Cover Pass FN	Cover Pass DPH	FBR DPH
2205/2209/A36, 1.57 kJ/mm	25	275	25–45	250	95	260	350
2.60 kJ/mm	23	250	25–45	230	95	245	280
2205/625/A36, 1.57 kJ/mm	0	220	0	205	0	200	210
2.60 kJ/mm	0	240	0	200	0	195	210

pass. Generally, the distance between indents was 0.5 mm (0.02 in.) in the lower passes of the weld, 1.0 mm (0.04 in.) in the central portions of the weld metal and 2.0 mm (0.12 in.) in the cover pass of the weld metal. Hardness was also measured along the fusion boundary and across the heat-affected zone (HAZ) into the base metal.

Hardness testing was also conducted at reduced loads (25 and 50 g) along the 2209/A36 and 625/A36 fusion boundaries. This was done to more closely examine the hardness in the microstructural transition region between the weld fusion zone and HAZ.

Ferrite Number Measurement

The ferrite number (FN) in each weld layer was determined using a Magne-Gage calibrated per AW5 A4.2-91 according to the method developed by Kotecki (Ref. 8). All measurements were obtained on longitudinal sections in the fusion zone rather than transverse sections in order to better quantify variation within a given pass. Four measurements were taken at four different locations within each pass. These measurements were then averaged to obtain the FN for each pass.

Charpy Impact Toughness Testing

Charpy V-notch (CVN) specimens were machined from the welded coupons. Samples were prepared in the L-T orientation as per ASTM E-23. The L-T orientation represents a sample transverse to the welding direction with the notch located such that testing occurs through the thickness of the weld from the root to the cover passes. All notches were located in the center of the weld deposit. Charpy V-notch testing was performed at temperatures from –196°C (–320.8°F) to more than 100°C (212°F) in order to develop a complete ductile-to-brittle transition temperature (DBTT) curve for each combination. Scanning electron microscopy (SEM) was utilized to examine the fracture surfaces of the CVN impact samples.

Pitting Corrosion Testing

Pitting corrosion tests were performed at 50°C (122°F) as described in ASTM G-48. Two types of samples were tested. The first type consisted of an entire weldment, including both base materials and the fusion zone. The second type was an all-weld-metal sample machined out of the fusion zone through the thickness. Since the thickness of the material was 12.5 mm, standard 25 x 50 mm (1 x 2 in.) specimens could not be used, and samples of 12.5 x 33.0 mm (0.5 x 1.3 in.) were used. The specimens were ground through 600-grit SiC and weighed prior to immersion in the solution. The pitting corrosion solution was 6% $FeCl_3 \cdot 6H_2O$. The specimens were immersed in this solution for 72 h and were removed and observed every 12 h to note any changes. Following the 72-h test period, the samples were carefully scrubbed under running water and then ultrasonically cleaned in methanol for approximately 30 min.

Evaluation of pitting was determined by optical microscopy. The pits were counted at magnifications of 50X and measured at 400X. Pit density was determined by dividing the number of pits per unit area. A pit density was determined for each weld layer so a comparison could be made between the different base material combinations and the heat input variations.

Results

2205/2209/A36 Weldment

Microstructure

The dissimilar 2205/A36 combination

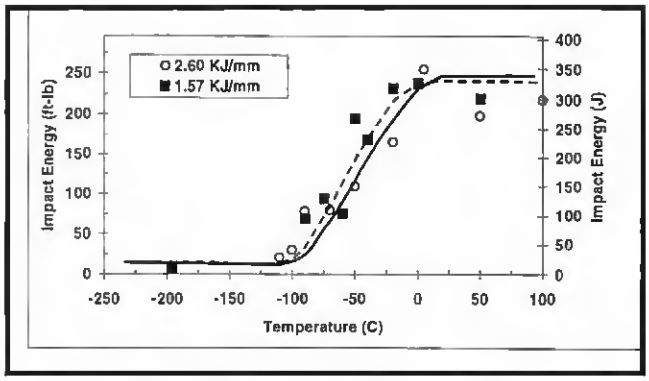

Fig. 7 — Charpy V-notch impact toughness vs. temperature for the 2205/2209/A36 weld combination.

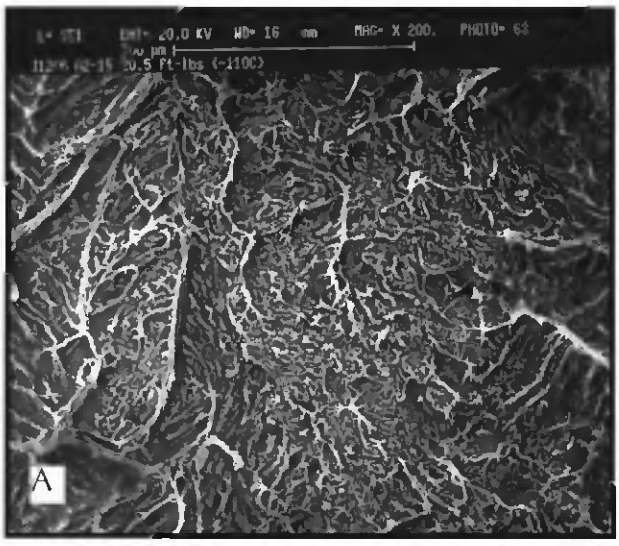

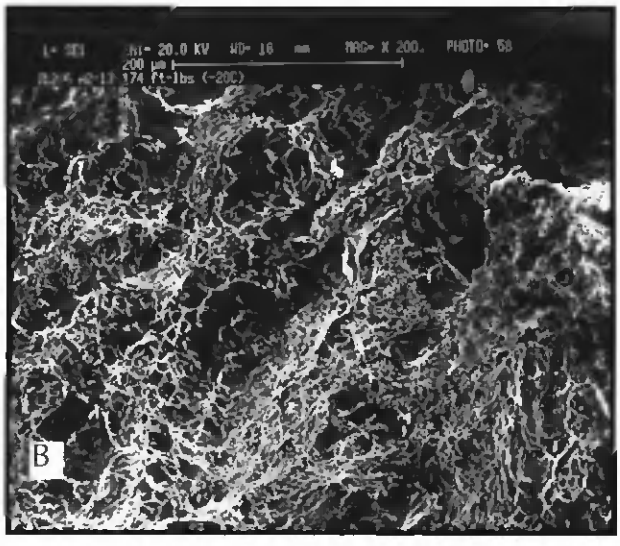

Fig. 8 — CVN fracture behavior for 2205/2209/A36 weldment: A — Lower shelf; B — fracture transition range.

was welded with duplex filler metal ER2209. Figure 3A shows the root pass microstructure of this combination resulting from a heat input of 1.05 kJ/mm and consists of an austenite matrix (white) with both skeletal and acicular ferrite (dark etching). Ferrite measurements indicated 20–25 FN in the root pass for both welding heat inputs of 1.57 KJ/mm and 2.60 KJ/mm. Based on this FN level, the WRC-1992 diagram (Fig. 4) predicts that the dilution in the root pass was approximately 33%, which corresponds well with the 35–40% dilution that was estimated metallographically. Subsequent passes in these weldments exhibited increased FN from the root to the cover pass, ultimately reaching 92 FN. A micrograph of the cover pass is shown in Fig. 3B. The FN transition from the root to the cover pass is shown in Fig. 5. Note that the FN differential between the root pass and cover pass is roughly 70 FN and that a significant increase in FN occurs between the last fill pass and the cover pass for both heat inputs.

The filler metal composition, dilution and cooling rate are the principal factors that influence the weld metal ferrite/austenite balance in duplex stainless steels. The lower heat input (1.57 kJ/mm) weld passes undoubtedly resulted in higher cooling rates than the higher heat input (2.60 kJ/mm) weld. However, as shown in Fig. 5, the difference in heat input and cooling rate did not significantly affect the ferrite/austenite balance. The major microstructural difference between these welds was that the lower heat input conditions resulted in the precipitation of more chromium nitride, presumably Cr_2N, within the ferrite phase. This precipitation was most pronounced in the cover pass. The layers beneath the cover pass exhibited greater volume fractions of austenite, which would therefore reduce the tendency for Cr_2N precipitation because austenite has a higher solubility for nitrogen than does the ferrite phase. The other major difference between the two heat input levels was the level of secondary austenite (γ_2). Both welds contained significant γ_2 in the fill passes beneath the cover pass. This γ_2 formation occurs due to reheating of weld metal during subsequent weld passes. This reheating and precipitation of γ_2 alters the ferrite/austenite volume fraction relative to that of the initial weld deposit.

Fusion Zone Hardness.

The resultant weld deposit hardness of this combination varied with heat input. The lower heat input weld exhibited higher hardness in the weld metal and along the A36 fusion boundary than the high heat input weld. The hardness in the root pass varied from 261 to 287 DPH . The remainder of the weld metal exhibited hardness levels between 229 and 279 DPH. An average hardness of 260 DPH was found in the cover pass. Lower hardness was found in the center portions of the fusion zone (midway through the thickness), as average hardness was 250 DPH. The hardness along the fusion boundary of the carbon steel was found to be much higher than the bulk fusion zone hardness and ranged from 253–416 DPH. Generally, the hardness along the 2209/A36 fusion boundary was above 300 DPH, with average levels reaching 410 DPH near the root pass. Softer regions along this boundary were found to exist in the top third of the weld. Average hardness levels within and at the fusion boundary of the A36/2209/2205 weldments are summarized in Table 4.

The 2.60-kJ/mm weld exhibited a lower average hardness, with root pass values from 249 to 256 DPH and an average hardness of 250 DPH (Table 4). The remainder of the weld metal exhibited hardness levels between 223 and 265 DPH. An average hardness of 245 DPH was measured in the cover pass. Lower hardness was found in the center portions of the fusion zone (midway through the thickness), with an average hardness of 230 DPH. The hardness along the 2209/A36 fusion boundary in this weld was also significantly lower than the lower heat input weld. The fusion boundary region associated with the root pass exhibited the highest hardness, 300

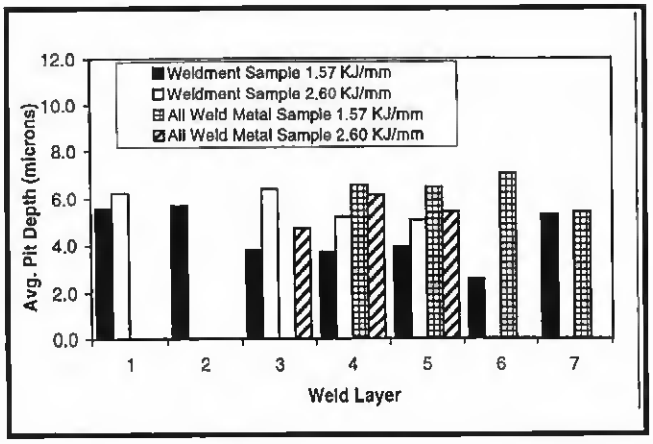

Fig. 9 — Average pit depth vs. weld layer for 2205/2209/A36 combination.

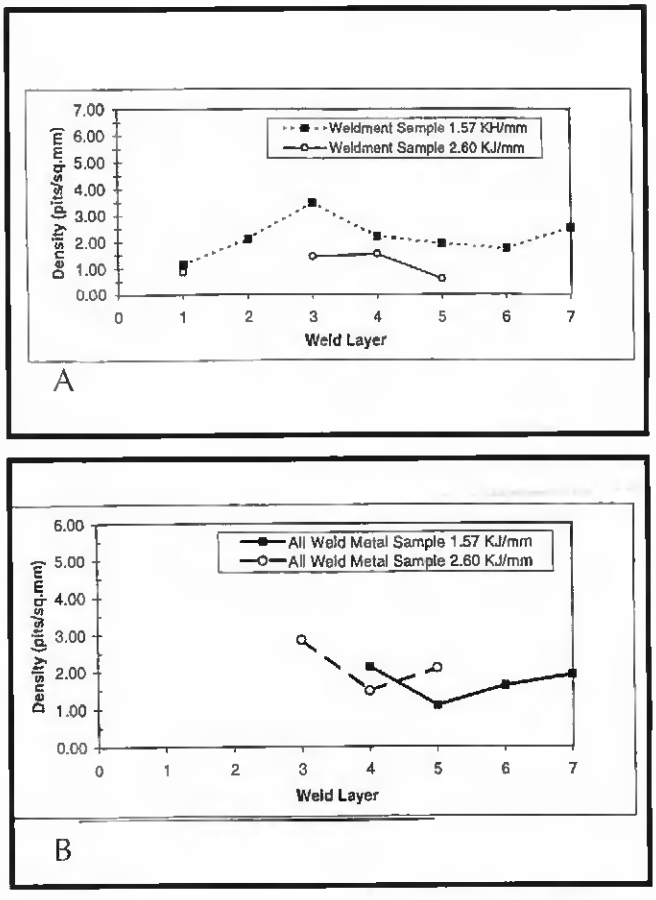

Fig. 10 — Pit density vs. weld layer for the 2205/2209/A36 pitting samples: A — Weldment samples; B — all-weld-metal samples.

DPH. Hardness elsewhere along the boundary was below 300 DPH with the lowest hardness exhibited in the fusion boundary adjacent to the cover pass.

A representative microstructure along the 2209/A36 fusion boundary region is shown in Fig. 6. This micrograph clearly shows an acicular martensitic structure, which results in significantly greater hardness along the 2209/A36 fusion boundary than along the 2205 fusion boundary. The carbon steel average base metal hardness (155 DPH) and the fusion boundary hardness (250–410 DPH) transitions rapidly within a short distance from the fusion boundary. Type II grain boundaries (Ref. 13) are also present along this fusion boundary. Type II boundaries have been previously reported by Wu and Patchett (Ref. 13) in nickel-based alloy cladding on Cr-Mo steels. Carbide precipitation decorates these boundaries resulting from carbon migration out of the carbon steel into the more highly alloyed, but lower carbon, fusion zone.

Weld Metal Impact Toughness

The CVN impact toughness results for the 2205/2209/A36 weld combination at both heat input levels are shown in Fig. 7. The lower shelf impact energy was roughly 7.5 ft-lb at temperatures below –140°C (–220°F). The upper shelf of the DBTT curve was roughly 240 ft-lb (325 J) for the 1.57 kJ/mm heat input and 250 ft-lb (339 J) for the 2.60 KJ/mm heat input. These DBTT curves also show the transition impact energy, midpoint between the upper and lower shelf, to be 125–130 ft-lb (169–176 J) and the corresponding transition temperature to be between –45 to –50°C (–49 to –58°F) for both heat input levels.

Fracture surfaces from upper and lower shelf and transition region specimens were evaluated in the SEM. The upper shelf fracture surface exhibited ductile fracture, as exemplified by a dimple-type fracture morphology. The lower shelf exhibited a cleavage-type fracture showing a relatively flat fracture surface

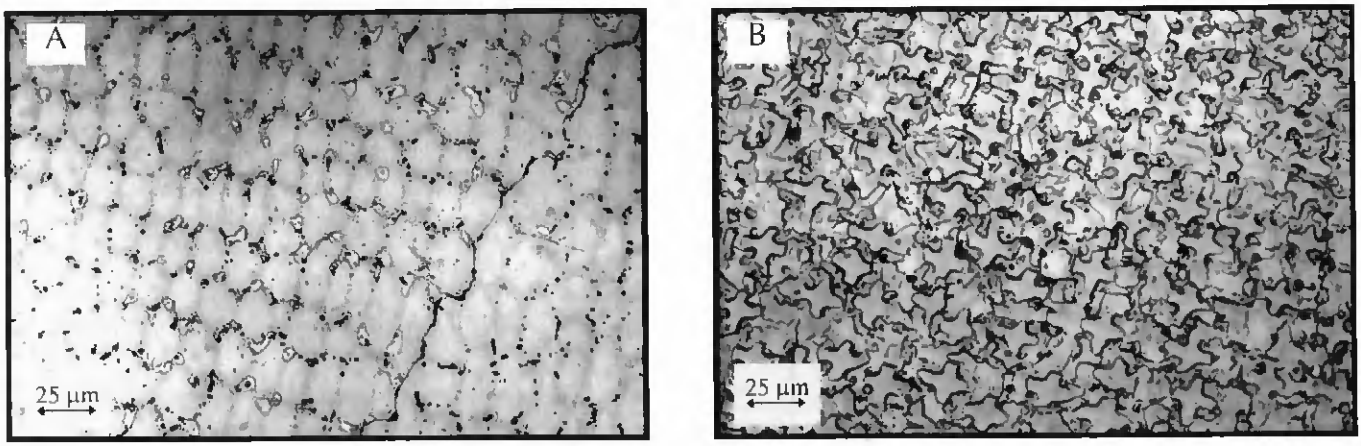

Fig. 11 — Microstructure of 2205/625/A36 combination: A — Root pass; B — cover pass.

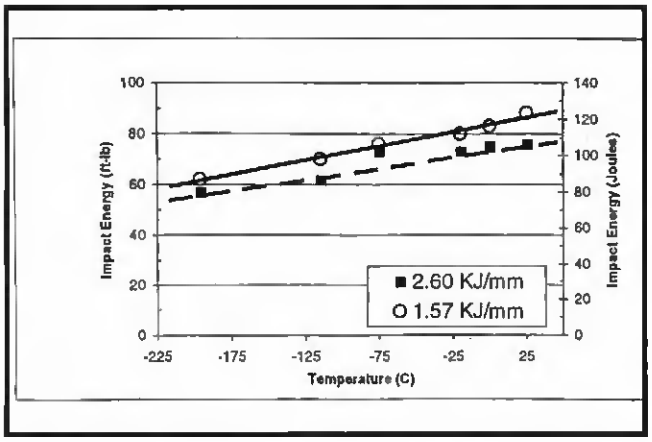

Fig. 12 — CVN impact toughness vs. temperature for the 2205/625/A36 weld combination.

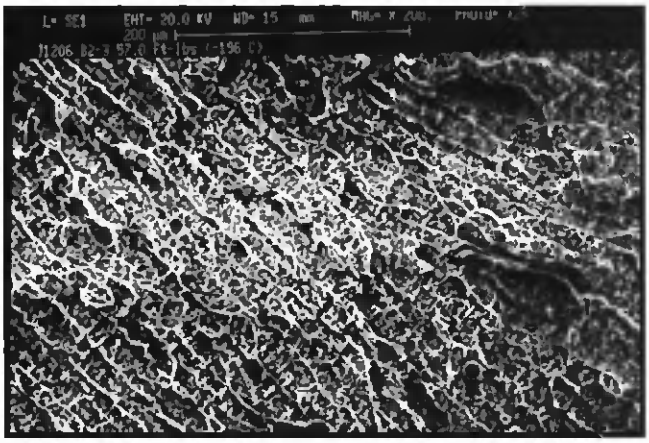

Fig. 13 — SEM fractograph of 2205/625/A36 CVN specimen produced at 1.57 kJ/mm and tested at –196°C.

as shown in Fig. 8A. Fracture surfaces in the transition region exhibited mixed mode fracture as shown in Fig. 8B. Portions of the fracture surface resemble cleavage fracture, while other areas show ductile fracture. The transition region fracture behavior was similar for both heat inputs in the temperature range from –20 to –90°C (–4 to –130°F).

Pitting Corrosion

Corrosion testing of the weld metal was conducted in two ways. Initial testing was conducted on the entire weldment by immersing the entire joint cross section, including the base materials, into 6% $FeCl_3$ solution at 50°C for 72 h. The second pitting corrosion test was conducted on all-weld-metal samples machined from the weldment. The pitting corrosion results were tabulated as pit density and average pit depth for the fusion zone.

In the weldment sample, the carbon steel was preferentially attacked by the solution, resulting in complete dissolution of the A36 base metal. The fusion zone pitting corrosion response varied with heat input and corrosion sample. The average pit depth of the weldment sample increased as the heat input increased, as shown in Fig. 9. Conversely, the average pit depth of the all-weld-metal samples decreased as the heat input increased. However, this relation is true only in weld layers 4 and 5 since the general attack experienced by the samples caused surface collapse in the initial passes of both heat input welds.

The weldment corrosion samples showed a decrease in pit density in the 2.60 kJ/mm weld as compared to the 1.57 kJ/mm weld. This is illustrated in Fig. 10A and shows that this relation holds true for all weld layers with the exception of the second pass due to accelerated attack in this layer. The 2.60 kJ/mm weld shows densities below 2.0 pits/mm^2 for all weld layers, while the lower heat input weld reveals densities generally greater. The all-weld-metal corrosion sample results are shown in Fig. 10B. General attack caused the surface collapse of the initial layers preventing data collection.

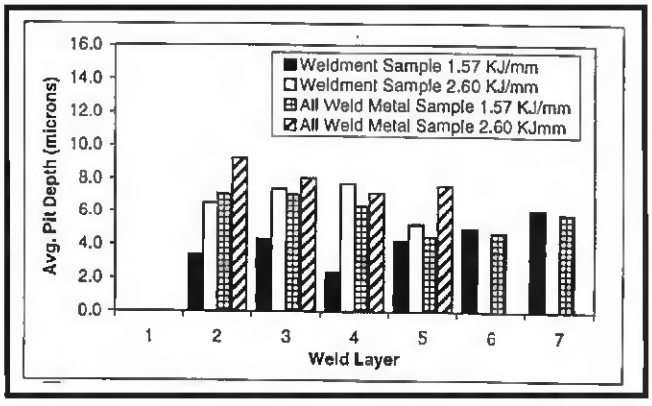

Fig. 14 — Average pit depth vs. weld layer for 2205/625/A36 combination.

Figure 10B also shows that no simple correlation can be drawn from the graph as pit density appears scattered between the two heat inputs. The weight loss measurements showed that the lower heat input weld resulted in greater weight loss than that of the higher heat input weld. The weight losses were 2.529 g (36.5% of initial weight) and 2.374 g (30.9% of initial weight) for the 1.57 and 2.60 kJ/mm weldments, respectively, thus indicating higher pitting corrosion resistance of the higher heat input weld.

2205/625/A36 Weldment

Microstructure

The dissimilar combination of Alloy 2205 and A36 was also welded using the Ni-based filler metal 625. The heat inputs utilized for fill and cover passes were the same as for the 2205/2209/A36 combination. The root pass heat input, 1.90 kJ/mm, was different from the 2205/2209/A36 combination due to differences in thermal properties of the filler alloys. Alloy 625 filler metal is a Ni-Cr-Mo material and consists nominally of 65% Ni, 20–23% Cr and 8–10% Mo. This alloy solidifies entirely to austenite with some possible lower melting point eutectic and/or carbide formation at the dendrite interstices. The root pass microstructure of this dissimilar weld joint is shown in Fig. 11A. It is fully austenitic with second phase constituents forming in the dendrite interstices. The cover pass of the 2205/625/A36 combination is shown in Fig. 11B. This fully austenitic microstructure is representative of that of the fill passes and exhibits a more distinct weld solidification substructure than the root pass. This difference results from the higher dilution of the filler metal by the base materials in the root pass.

Fusion Zone Hardness

The fusion zone hardness for the 2205/625/A36 welds was unaffected by weld heat input, ranging from 190–220 DPH. Similarly, the hardness along the

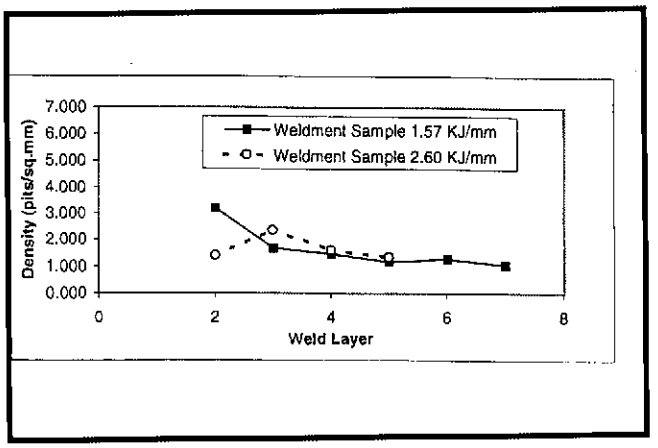

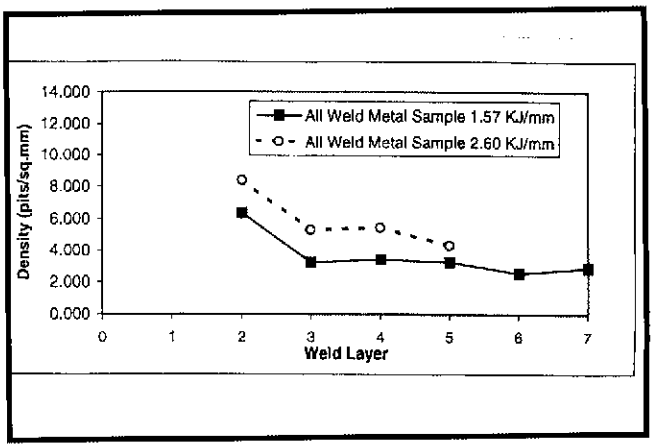

Fig. 15 — Pit density vs. weld layer for 2205/625/A36 combination: A — Weldment sample; B — all weld metal.

Table 5 — CVN Data for the Various Dissimilar Combinations

Combination	Upper Shelf (ft-lb)	Lower Shelf (ft-lb)	Transition Region °C	Transition Region Energy (ft-lb)
2205/2209/A36, 1.57 kJ/mm	240	7.5	−50	124
2.60 kJ/mm	250	7.5	−45	129
2205/625/A36, 1.57 kJ/mm	79 @ 25°C	57 @ −196°C	NA	NA
2.60 kJ/mm	88 @ 25°C	63 @ −195°C	NA	NA

Table 6 — Comparison of CVN Impact Toughness Relative to Previous Work

Combination	CVN, R.T. ft-lb	CVN, R.T. Joules	CVN, −40°C ft-lb	CVN, −40°C Joules
2205/2209/A36, 1.57 kJ/mm	250	339	150	203
2.60 kJ/mm	240	325	170	230
2205/625/A36, 1.57 kJ/mm	88	119	80	108
2.60 kJ/mm	79	107	73	99
Kotecki (Ref. 16) ER2209	160	217	115	156
Bonnefois (Ref. 17) ER2209	192	260	133	180

carbon steel fusion boundary region was comparable to that of the fusion zone for both heat inputs, ranging from 180–220 DPH. The average hardness values for this combination are also summarized in Table 4.

Weld Metal Impact Toughness

Charpy V-notch test results for the 2205/625/A36 dissimilar weld combination are shown in Fig. 12. As expected, a DBTT is not observed due to the fully austenitic structure of the fusion zone. The impact toughness decreases slightly with decreasing temperature. At −196°C impact toughness was 62 ft-lb (84 J) and 57 ft-lb (77 J) for 1.57 kJ/mm and 2.60 kJ/mm heat inputs, respectively, relative to 88 ft-lb (119 J) and 76 ft-lb (103 J) at 25°C (77°F). Note that the lower heat input, 1.57 kJ/mm, resulted in higher impact toughness values at any given temperature. A representative fracture surface for this combination is shown in Fig. 13. The fracture mode was ductile rupture over the entire range from −196°C to 25°C. Note the evidence of the underlying solidification substructure on this fracture surface, probably due to fracture initiation at the interdendritic eutectic constituent.

Pitting Corrosion

The weldment corrosion response of the 2205/625/A36 weldments also resulted, as expected, in general attack of the carbon steel base metal. Attack was also very pronounced in the root of the weld and resulted in the complete dissolution of the root pass. The root pass was the only pass attacked in this manner and probably resulted from higher dilution of this pass by the A36 base metal. Figure 14 shows increased pit depths with increased heat input for both corrosion sample types. However, the pit depth difference is much smaller in the all-weld-metal samples than the weldment samples when comparing the two heat inputs. The pitting density results vs. weld layer for the weldment and all-weld-metal samples are shown in Fig. 15. Pit density increased with increased heat input as shown for both corrosion samples. The only exception is weld layer 2 in the weldment sample, as the higher heat input resulted in lower pit density relative to the 1.57 kJ/mm weld. The pit densities of both corrosion sample types appear higher in the initial weld layers and generally tend to level out above the third weld layer.

The weight loss of the all-weld-metal corrosion samples was 1.402 g (21.5% of initial weight) and 2.212 g (20.6% of initial weight) for the 1.57 kJ/mm and 2.60 kJ/mm heat inputs, respectively. The corrosion rate, expressed as weight percent, indicates that no difference in pitting corrosion is evident between the two heat inputs as the weight loss percentages result in similar values.

Discussion

The results of this investigation have shown that duplex stainless steel alloy 2205 can be joined to A36 carbon steel using either duplex filler material ER2209 or Ni-based Alloy 625. Both combinations exhibited good weldability and were free from fabrication-related defects such as solidification cracking, liquation cracking, porosity, incomplete fusion, etc. In general, from a procedural point of view, there were no problems welding the dissimilar combinations using either filler material.

Microstructure Evolution

Weld Metal

Table 4 compares the FN and hardness for each of the combinations studied relative to location in the weld, *i.e.* root pass, fill passes and cover pass. Dilution

Table 7 — Pitting Corrosion Data for the Weldment and All-Weld-Metal Samples

Combination	Root Pass Density (pits/mm²)	Root Pass Depth (μm)	Fill Pass Density (pits/mm²)	Fill Pass Depth (μm)	Cover Pass Density (pits/mm²)	Cover Pass Depth (μm)
2205/2209/A36						
Weldment, 1.57 kJ/mm	1.15	5.55	2.30	3.91	2.53	5.94
2.60 kJ/mm	0.89	6.21	1.49	5.78	1.13	5.62
Weld Metal, 1.57 kJ/mm	—	—	1.61	6.67	1.90	5.39
2.60 kJ/mm	—	—	2.16	5.41	2.08	5.40
2205/625/A36						
Weldment, 1.57 kJ/mm	—	—	1.75	3.84	1.04	6.04
2.60 kJ/mm	—	—	1.77	7.18	1.33	5.24
Weld Metal, 1.57 kJ/mm	—	—	3.74	5.91	2.86	5.82
2.60 kJ/mm	—	—	6.36	8.13	4.30	7.58

Table 8 — Weight Loss from the All-Weld-Metal Corrosion Samples

All-Weld-Metal Corrosion Samples Combination	Weight Loss grams	Weight Loss wt-%
2205/2209/A36,		
1.57 kJ/mm	2.529	36.5
2.60 kJ/mm	2.374	30.9
2205/625/A36,		
1.57 kJ/mm	1.402	21.5
2.60 kJ/mm	2.212	20.6

of the Alloy 625 filler metal is not sufficient to form ferrite within the weld deposit, and the entire fusion zone is austenitic. The 2205/2209/A36 weld exhibited 20–25 FN in the root pass, 25–45 FN in the fill passes and increased significantly to 95 FN in the cover pass. The fill passes showed a gradual increase in FN with each pass. This results from both a change in dilution from bottom to top in the multipass weld and the formation of secondary austenite in underlying weld passes that reduces the FN in the underlying passes. The WRC-1992 diagram can be used to estimate the dilution effects on FN, but the diagram is not effective in predicting secondary austenite formation in multipass welds. Thus, some deviation from the predicted WRC-1992 FN based strictly on dilution calculations would be expected. In addition, this diagram predicted lower FN for the cover pass than was actually measured.

The cover pass FN increased significantly relative to the last fill pass for the 2205/2209/A36 combination. It is interesting to note that the cover pass ferrite number (95 FN) is actually greater than the predicted FN of undiluted ER2209 filler metal. The reason for this high FN in the cover pass is not clear. The fact that the cover pass FN is comparable between heat inputs suggests that cooling rate is not a factor. Previous researchers have suggested that the fusion zone austenite content is not strongly dependent on heat input, and is controlled primarily by the composition of the weld metal (Refs. 9–11). Composition analysis of the individual passes was not performed and, thus, it is not apparent what composition difference may exist between the fill passes and cover passes. The formation of secondary austenite in the underlying fill passes may explain some of the difference, but does not help rationalize why the cover pass FN exceeds that calculated from the filler metal composition. The loss of an austenite forming element, such as nitrogen, may explain the difference, but was not verified.

The root pass of both weld combinations exhibited slightly higher hardness than the fill passes. In the 2205/2209/A36 combination, this may be due to higher levels of secondary austenite (γ_2) formation during reheating by the subsequent passes. The intragranular precipitation of γ_2 results in some second phase strengthening and thus a small increase in hardness. The increase in hardness in the cover pass results from the high Cr_2N precipitate concentration associated with highly ferritic weld metals. The hardness increase is particularly pronounced in the low heat input weld cover pass — Table 4.

The 2205/625/A36 weld combination exhibited a fully austenitic fusion zone and, hence, there was little change in hardness through the weld thickness. Slightly higher hardness in the root pass of this combination may be attributed to higher dilution from the base materials and reflects the difference in microstructure between the root and fill passes.

Fusion Boundary Region Microstructure

The high hardness along the fusion boundary region of both weld combinations is attributable to the formation of a narrow band of martensite at the dissimilar interface. This martensitic region is predicted in both cases by the Schaeffler Diagram — Fig. 1. By drawing tie lines between the filler metal composition and midpoint of the base metal compositions, it can be seen that for the 2209/625/A36 combination, 15% of this tie line lies within a region where martensite is present. The 2205/2209/A36 tie line, on the other hand, has more than 65% of its length in a martensitic region. Thus, for the 2209 filler metal the composition transition region over which martensite can form will be much wider. This may explain the pronounced martensite formation along the 2205/2209/A36 fusion boundary region and the apparent martensite-free fusion boundary region in the 2205/625/A36 weld. Another factor that influences martensite formation is the difference in carbon diffusion rates in the different combinations. If carbon migration is reduced or restricted, the likelihood of martensite formation will be similarly reduced.

Gittos and Gooch (Ref. 12) studied the fusion boundary below stainless steel and nickel-alloy claddings on Cr-Mo steels. They reported narrow bands of martensite formation along the interfaces of both cladding alloys, with hardness levels in the as-welded condition ranging from 300–441 HV. This martensitic band was associated with the partial mixing region between the fusion zone and base metal HAZ.

It is interesting to note in Fig. 6 that Type II grain boundaries are present within the fusion zone. Wu and Patchett (Ref. 13) found similar Type II grain boundaries previously in austenitic stainless steel cladding. They reported that Type II grain boundaries were formed due to the crystallographic change from δ-ferrite, the existent phase of solid hypoperitectic base steel at the initial transient of solidification, to γ-austenite as a result of accumulation of nickel at the solidification front. They reported that disbonding (*i.e.*, cracking) was more severe in nickel-based alloy deposits that solidified directly to austenite where high dilution from the base metal was incurred. However, they also claimed that the ferritic solidification of duplex stainless steels eliminates Type II grain boundaries from occurring. This may suggest that the solidification behavior in this partially mixed region adjacent to the fusion boundary may be different from that of the bulk fusion zone, or that solid-state transformations following solidification may result in the formation of these boundaries. The nature of the Type II boundaries is the subject of ongoing research (Ref. 14).

Toughness Behavior

The CVN results for both combinations are summarized in Table 5. In the 2205/2209/A36 combination, there was little apparent difference in toughness as a function of heat input, which reflects the similarity in microstructure of these

weld deposits. Because of the L-T orientation of the test samples, the toughness values represent a composite of the entire weld deposit and are not indicative of local variations due to microstructure. For example, lower toughness might be expected in the higher FN cover pass.

It should be pointed out that the toughness of the 2205/2209/A36 may be significantly affected by the formation of martensite along the A36 fusion boundary region. This narrow band of martensite would undoubtedly result in reduced toughness along this particular region relative to the fusion zone. However, no fusion boundary CVN testing was performed to investigate any toughness anomaly in this region.

As expected, the fully austenitic fusion zone of the 2205/625/A36 combination exhibited good impact toughness over a wide range of temperatures. This microstructure does not exhibit upper/lower shelf transition behavior such as ferritic (or high ferrite) weld metals, and, instead, the impact toughness exhibits a gradual decrease with temperature. It is interesting that the upper shelf toughness of the duplex 2209 deposit far exceeds that of the Alloy 625 deposit and that the duplex filler material provides comparable toughness at temperatures down to –60°C.

Table 6 compares fusion zone impact energies obtained in this study to previous work from duplex stainless base/filler metal combinations performed by Kotecki (Ref. 15) and Bonnefois, *et al.* (Ref. 16). The impact toughness data reported here are higher than from this previous work and may be attributed to higher austenite contents (lower FN) in the root and fill passes of the dissimilar welds. Most importantly, these comparisons suggest that dilution from a dissimilar carbon steel base metal does not compromise the toughness of the fusion zone relative to a similar metal combination.

Corrosion Behavior

The two types of corrosion samples (weldment and all weld metal) and their pitting corrosion data are summarized in Table 7. As shown for the 2205/2209/A36 material combination, the weldment sample shows that for increasing heat input, the pitting corrosion resistance increased when considering the pit density. The average pit depth, on the other hand, increased with increasing heat input and may be due to higher concentration on fewer initiated pits. Yasuda (Ref. 17) and Ume (Ref. 18) claim that pitting corrosion decreases with increased heat input due to slower cooling rates and the formation of austenite rather than Cr_2N precipitation within the ferrite phase of the fusion zone. Another beneficial effect of lower cooling rates on pitting resistance is the healing of chromium-depleted regions around any precipitates. Ume (Ref. 18) reported that the number of initiation sites decrease with higher heat inputs, thereby supporting the data collected in the current study of the weldment samples.

The all-weld-metal samples exhibited increased pit density and depth for the higher heat input relative to the 1.57 kJ/mm weld. However, the all-weld-metal corrosion data may be erroneous due to the collapse of the surface in many of these samples, thereby changing the kinetics of the corrosion testing relative to the weldment samples.

Table 8 compares the weight loss due to corrosion of the all-weld-metal samples. The percentage weight loss illustrates that increased corrosion resistance is obtained with increased heat input for the 2205/2209/A36 combination. Sridhar, *et al.* (Ref. 19), showed that pitting corrosion resistance, expressed as a percentage of weight loss, increases with higher heat inputs. They claimed that slower cooling rates resulting in increased austenite and the distribution of the various elements between the ferrite and austenite are the reasons for the increased pitting resistance.

The 2205/625/A36 combination resulted in the localized attack of the root pass in each of the corrosion samples tested. The root pass of the all weld metal corrosion samples was completely dissolved by the ferric-chloride solution. This is apparently the result of higher dilution of the filler metal by the carbon steel, as indicated by a variation in microstructure relative to the subsequent corrosion-resistant fill passes. This suggests that a critical composition change occurs between the root pass and the remaining fill and cover passes.

Summary and Recommendations

The 2205/A36 base metal combination has been successfully joined with duplex stainless steel ER2209 and Ni-based Alloy 625 filler metals using multipass GTAW. Heat input had only a minor effect on the microstructure and toughness for the ER2209 combination. However, the corrosion behavior showed a marked improvement for higher heat input welding parameters relative to the lower heat input.

The choice of filler metals in joining 2205 to A36 will be primarily dependent on the service requirements needed. The strength and ductility of nickel-based Alloy 625 and duplex filler metal ER2209 are similar, being roughly 110 ksi and 30–40% elongation. Therefore, a balance between toughness and corrosion resistance will determine the use of either the duplex filler metal ER2209 or the nickel-based Alloy 625. The recommendation for cryogenic temperatures would be to utilize Alloy 625 over the duplex filler metal due the increased toughness at these temperatures. However, dilution should be minimized in the root pass to limit the carbon steel dilution in the fusion zone to prevent the reduction in corrosion resistance. On the other hand, in service environment temperatures greater than –50°C, the duplex filler metal ER2209 should be utilized due to higher toughness over the nickel-base Alloy 625. The heat input should be as high as possible in order to gain the maximum corrosion resistance of the fusion zone.

Conclusions

1) The fusion zone microstructures of dissimilar weld combination 2205/2209/A36 resulted in a general increase in ferrite number with each subsequent pass and a large increase in FN occurred between the last fill pass and the cover pass. The measured FN in the cover pass was greater than that predicted by the WRC-1992 diagram.

2) The ferrite number and hardness of the 2205/2209/A36 combination were similar for both the 1.57 and 2.60 kJ/mm heat inputs, suggesting that heat input is a secondary factor relative to weld metal composition in controlling the ferrite/austenite phase balance.

3) The 2205/2209/A36 combination formed a narrow martensitic band adjacent to the A36 fusion boundary along the entire thickness of the weld. No martensite was observed in welds made with the Alloy 625 filler metal, possibly due to the smaller composition range over which martensite forms and lower carbon migration rates in Ni-based vs. Fe-based alloys.

4) The 2205/2209/A36 fusion zone exhibited similar upper shelf energies for the two heat inputs utilized, suggesting that heat input and dilution from the dissimilar base metal had little or no effect on the mechanical properties.

5) The 2205/625/A36 fusion zone toughness behavior was typical of face-centered cubic (FCC) materials as impact energies decreased 10–15 ft-lh (14–20 J) over a temperature range from 25° to –196°C.

6) Pitting corrosion resistance of the weldment samples utilizing 2209 filler metal showed increased resistance as the heat input increased from 1.57 kJ/mm to 2.60 kJ/mm. The all weld metal samples

resulted in a lower percentage weight loss for the higher heat input weld, signifying increased corrosion resistance with the 2.60 kJ/mm weld relative to the 1.57 kJ/mm weld.

7) The Alloy 625 fusion zone exhibited general attack in the root pass for each type of corrosion sample tested. It appeared that corrosion resistance of the 2205/625/A36 combination decreases with increasing heat input for the remaining fill and cover passes.

Acknowledgment

This work was supported by the members of Edison Welding Institute through the Cooperative Research Program. The technical support of Dr. Wangen Lin, formerly with EWI and currently with Pratt & Whitney, and other members of the EWI staff during the course of this investigation is greatly appreciated.

References

1. Pattee, H. E., Evans, R. M., and Monroe, R. E. 1968. *The Joining of Dissimilar Metals.* Defense Metals Information Center, Battelle Memorial Institute, Columbus, Ohio.

2. Schaeffler, A. L. 1949. Constitution diagram for stainless steel weld metal. *Metal Progress* 56(11): 680–680B.

3. Long, C. J., and DeLong, W. T. 1973. The ferrite content of austenitic stainless steel weld metal. *Welding Journal* 52(7): 281-s to 297-s.

4. Siewert, T. A., McCowan, C. N., and Olson, D. L. 1988. Ferrite Number prediction to 100 FN in stainless steel weld metal. *Welding Journal* 67(12): 289-s to 298-s.

5. Kotecki, D. J., and Siewert, T. A. 1992. WRC-1992 Constitution Diagram for stainless steel weld metals: a modification of the WRC-1988 Diagram. *Welding Journal* 71(5): 171-s to 178-s.

6. Odegard, L., Pettersson, C. O., and Fager, S. A. 1994. The selection of welding consumables and properties of dissimilar welded joints in the superduplex stainless steel Sandvik 2507 to carbon steel and highly alloyed austenitic and duplex stainless steels. *Proceedings of the 4th International Conference of Duplex Stainless Steels*, Glasgow, Scotland, Paper No. 94.

7. Nelson, D. E., Baeslack, W. A., and Lippold, J. C. 1985. Characterization of the weld microstructure in a duplex stainless steel using color metallography. *Metallography* 18(3): 213–224.

8. Kotecki, D. J. 1982. Extension of the WRC Ferrite Number system. *Welding Journal* 61(11): 352-s to 361-s.

9. Honeycomb, J., and Gooch, T. G., 1985. Arc welding ferritic-austenitic stainless steels: prediction of weld area microstructures. The Welding Institute Research Report, 286/1985.

10. Gooch, T. G. 1982. *Proc. Conf. Duplex Stainless Steels.* St Louis, published by ASM International, Materials Park, Ohio, 1983.

11. Mundt, R., and Hoffmeister, H. 1983. The continuous ferrite-austenite transformation during cooling of ferritic-austenitic iron-chromium-nickel alloys, *Arch. Eisenhuttenwes* 54, No. 7, pp. 291–294.

12. Gittos, M. F., and Gooch, T. G. 1992. The interface below stainless steel and nickel-alloy claddings. *Welding Journal* 71(12): 461-s to 472-s.

13. Wu, Y., and Patchett, B. M. 1994. Solidification microstructure and sources of Type II grain boundary disbonding in CRA cladding. Paper presented at 1995 AWS Annual Meeting, Cleveland, Ohio.

14. Nelson, T. W., Mills, M., and Lippold, J. C. 1998. Weld interface phenomena in dissimilar metal welds. Accepted for publication in *Science and Technology of Welding and Joining.*

15. Kotecki, D. J. 1990. *Weldability of Materials Conference Proceedings*, 127, Edited by R. A. Patterson and K. W. Mahin, ASM International, Materials Park, Ohio.

16. Bonnefois, B., Charles, J., Dupoiron, F., and Soulignac, P. 1991. How to predict welding properties of duplex stainless steels. *Proc. Duplex Stainless Steels '91*, Beaune, Bourgogne, France, Vol. 1, pp. 347–361.

17. Yasuda, K., Tamaki, K., Nakano, S., Kohayashi, K., and Nishiyama, N. 1986. Metallurgical characteristics of weld metals and corrosion performance of girth weld joints of duplex stainless steel pipes. *Duplex Stainless Steels*, ASM International, Materials Park, Ohio, p. 201.

18. Ume, K., Seki, N., Naganawa, Y., Hyodo, T., Satoh, K., and Kuriki, Y. 1987. Influence of thermal history on the corrosion resistance of duplex stainless steel linepipe. *Materials Performance*, No. 8, pp 25–31.

19. Sridhar, N., Flasche, L. H., and Kolts, J. 1984. Effect of welding parameters on localized corrosion of a duplex stainless steel. *Materials Performance*, pp 52–55.